Purcell Enhancement of Spontaneous Emission from Quantum Cascades inside Mirror-Grating Metal Cavities at THz Frequencies

Yanko Todorov,[1] Isabelle Sagnes,[1] Izo Abram,[1] and Christophe Minot[2,1]

[1]*CNRS/LPN, Laboratoire de Photonique et de Nanostructures, Route de Nozay, 91460 Marcoussis, France*

[2]*GET/Telecom Paris, 46 rue Barrault, 75634 Paris Cedex 13, France*

(Received 25 May 2007; published 29 November 2007)

Quantum cascade devices processed into double metal cavities with subwavelength thickness and a grating on top are studied at terahertz frequencies. The power extracted from the devices as a function of the device thickness and the grating period is analyzed owing to electrodynamical modeling of dipole emission based on a modal method in multilayer systems. The experimental data thus reveal a strong Purcell enhancement, with Purcell factors up to ≈ 50.

DOI: 10.1103/PhysRevLett.99.223603 PACS numbers: 42.50.Pq, 42.55.Px, 73.40.Sx, 78.67.Pt

E. M. Purcell [1] was the first to point out that spontaneous emission (SE) dynamics is modified when the source is placed inside a cavity with dimensions comparable to the wavelength λ. If the source is resonant with a cavity mode, the SE is enhanced by a factor $f = (3/4\pi^2)Q(\lambda^3/\mathcal{V})$ which is proportional to the ratio of the quality factor Q and the volume of the resonant mode $\mathcal{V}$. The Purcell effect has been first demonstrated in the microwave region for Rydberg atoms inside a high Q superconductor cavity [2]. In semiconductors, Purcell enhancement and inhibition have been evidenced in the optical domain [3], and the control of the dynamics has now become a workhouse for the design of more efficient and directional devices, as well as compact single photon [4] or entangled photon pair [5] sources for various quantum electrodynamics (QED) experiments.

In all the works cited above, the Purcell effect relies on cavities with fully tridimensional confinement of the mode, to provide low volume $\mathcal{V}$ and high Q factors. In planar microcavities, which are in closer connection with the usual laser devices, SE is also modified. In this case, the enhancement almost exclusively originates from the confinement of the electromagnetic field, rather than high Q factors. For horizontal dipoles (parallel to the mirrors), f does not exceed a few units in approximately half-wavelength microcavities [6]. However, for vertical dipoles (perpendicular to the mirrors), f is expected to increase as the ratio of the wavelength to the cavity thickness L, for example [7]:

$$f = \frac{3}{4n}\frac{\lambda}{L} \tag{1}$$

for a dielectric medium with refractive index n inside a single-mode planar cavity with perfectly conducting metallic mirrors. Then the confinement of the field in a strongly subwavelength microcavity can give rise to a very large enhancement of vertical dipole emission dynamics. This can be achieved in the long wavelength region of the optical spectrum, at terahertz (THz) frequencies, where intersubband transitions in semiconductor quantum wells provide large vertical dipoles, suitable for laser emission [8], and metallic mirrors exhibit excellent reflectivity at almost all incident angles.

In this Letter, we demonstrate the Purcell enhancement of the electroluminescence emitted by THz quantum cascade structures in metallic microcavities through the cavity thickness dependence of the SE rate. The photons are coupled out of the cavity by a rectangular slit metallic grating which also serves as an upper mirror. The interpretation of the results relies upon a detailed modeling of both the electromagnetic and electrodynamic properties of the dipole emission in the cavity, in order to distinguish between a static contribution to the emitted power, due to a grating period dependent extraction coefficient, and a dynamical contribution, due to the SE rate enhancement observed while reducing the cavity thickness.

In the experiments, the sources of THz radiation are $GaAs/Al_{0.15}Ga_{0.85}As$ quantum cascade (QC) devices grown by metalorganic chemical vapor deposition (MOCVD). The QC active region consists of N identical repetition modules, 92.5 nm thick, the detailed epitaxial structure of which is given in Ref. [9]. They are sandwiched between Si-doped contact layers with thicknesses 80 nm and 300 nm, and respective doping levels 2×10^{18} cm^{-3} and 3×10^{18} cm^{-3}. Identical layer stackings are grown in four distinct samples which only differ by the number of modules $N = 39$, 19, 9, and 4, and measured thickness 3.50 μm, 1.76 μm, 0.88 μm, and 0.44 μm, respectively, $\sim$5% less than nominal.

To obtain double metal cavities, the QC structures are bonded on host InP n^+ substrates. The bonding layer is an Au-In alloy with metallic properties and serves as the lower planar mirror of the cavity. After removal of the growth substrate by selective wet etching, 400 nm thick TiAu gratings with periods p ranging from 10 μm to 22 μm and 50% duty cycle are lithographically deposited, and 200×400 μm^2 wet etched rectangular mesas formed (Fig. 1, upper left panel). Finally, annealing at 350 °C

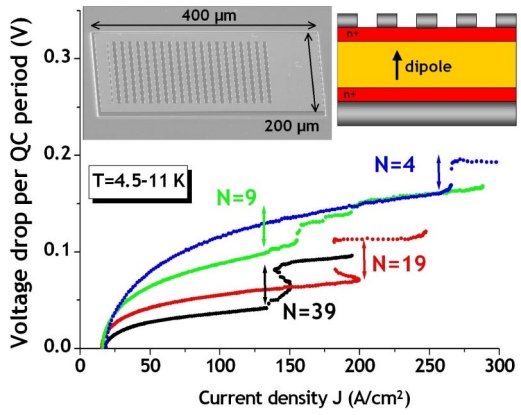

FIG. 1 (color online). Current-voltage characteristics for the four samples at $T = 4.5$–11 K. Upper left: electron microscope picture of a metal-bonded mesa with a grating on top. Upper right: schematic of the device. The active medium is modeled as a set of electrically excited dipole sources.

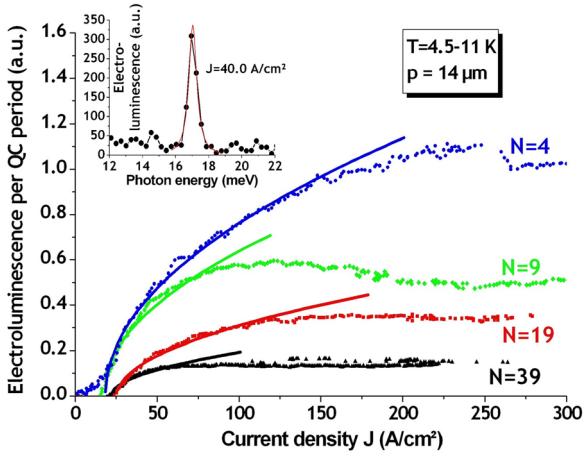

FIG. 2 (color online). Electroluminescence per QC period N as a function of the injected current in devices with a 14 μm period grating, for the four samples. The solid lines are square root fits according to Eq. (3). Inset: experimental spectrum of a $N = 39$ device at $T = 11$ K.

reduces the contact resistances while preserving very low scattering of long wavelengths at the metal-semiconductor interfaces. The top 80 nm contact layer lying just below the grating is thinner than the bottom one in order to minimize absorption of the out-coming radiation. In this grating-coupling scheme (Fig. 1, upper right panel) the generated THz power is extracted uniformly from the entire surface, rather than from the edge over an absorption length which depends on the cavity thickness. As shown in Fig. 1, a planar cavity is formed between both pairs of metallic and doped layers, which exhibit high reflectivity in the THz range (the plasma frequency is 17 THz for a doping concentration of 3×10^{18} cm^{-3}).

The devices are electrically and optically characterized between 200 and 4.5 K. Figure 1 shows the current-voltage characteristics of the devices at low temperature (4.5–11 K). The rectifying part of the characteristics (below $\approx$1 V) and the voltage drop caused by access resistances are removed, so that the curves can be scaled to one QC period. The rising edge is governed by the resonant tunneling effect responsible for the current injection into the upper state of the THz optical transition. In the thinner samples the resonance voltage is higher because the QC injectors are more depleted on the average, due to carrier diffusion into the contact layers. Above resonance, however, where a high field domain progressively extends over the whole QC, the width of the current plateau, about 40 meV, does not depend on the QC thickness (except for a slightly lower value in the $N = 4$ case). This indicates that, near resonance, similar injection conditions prevail over all the active regions, and all of the latter contribute to the THz emission equivalently.

Spectral measurements at low injection current (inset of Fig. 2) reveal a 0.5 meV wide emission line occurring at 17 meV, i.e., $\lambda = 73$ μm (4.3 THz). The cavity thicknesses are thus notably smaller than the wavelength in the semiconductor material, even for the thickest $N = 39$ devices. The narrow linewidth ($\Delta\lambda/\lambda \approx 3\%$) and the low level of background emission attest the excellent homogeneity of the MOCVD layers along the growth axis.

At THz frequencies the enhancement of the SE rate can be evidenced in cw experiments through the relative magnitude of the emitted intensities. This requires, however, that power losses and power collection effects do not conceal the dynamical origin of the enhancement. Therefore, measurements of the electroluminescence-current characteristics are performed at low temperature ($T \lesssim 10$ K) in order to investigate the cavity thickness dependence of the emitted power. Figure 2 shows the electroluminescence *per QC period* for a $p = 14$ μm period grating for the four samples. The extracted power per period clearly increases when the cavity thickness is reduced, approximately as $1/N$.

The power per QC period P/N radiated from the device through the grating can be written as:

$$\frac{P}{N} = \eta_{\text{ext}} \frac{\Gamma_{\text{sp}}}{\Gamma_{\text{nr}} + \Gamma_{\text{sp}}} \hbar\omega \frac{I}{e}, \tag{2}$$

where Γ_{sp} is the SE rate, Γ_{nr} is the rate of nonradiative transitions ($\Gamma_{\text{nr}} \gg \Gamma_{\text{sp}}$), $\hbar\omega$ is the photon energy, I the electric current, e the electron charge, and η_{ext} the extraction coefficient. In the experimental setup, the sample is placed at the entrance of a Winston cone and the optical signal is detected by a cooled Ge bolometer inside a photometer placed just in front of the cone. In this configuration, the radiation is collected from the sample in a large aperture estimated at about 120°, and η_{ext} is very close to the intrinsical extraction coefficient of the metallic grating, owing to the almost perfect extraction efficiency of the Winston cone [10].

The rate of nonradiative transitions Γ_{nr} is mainly governed by LO-phonon, interface roughness and electron-

electron scattering. In GaAs, the LO-phonon channel is blocked below 20 K for the transition energy $\hbar\omega = 17$ meV is lower than the phonon energy (36 meV). This is confirmed by the temperature dependence of the luminescence, which does not vary with T below 20 K and exponentially decays as a function of $1/T$ above [11]. While the interface roughness contribution to Γ_{nr} does not depend on the carrier density and the current, the remaining electron-electron contribution is proportional to the square root of the current [12]. As Fig. 2 shows, the results are satisfactorily reproduced if the electron-electron interaction mechanism is considered to be dominant [9], and at low temperature the radiated power per period is written in the form:

$$P/N = c\eta_{ext}\Gamma_{sp}\sqrt{I - I_0}\hbar\omega \quad (3)$$

with c a constant and I_0 the rectification current, apparent from Figs. 1 and 2. A square root fit of the radiated power versus current curve (Fig. 2) in the low injection region gets rid of the current dependence of the luminescence and yields the product $\eta_{ext}\Gamma_{sp}$.

In order to be conclusive on the relative variation of Γ_{sp}, the gratings with different periods are used as a probe of the extraction efficiency. The experimental results are summarized in Fig. 3 where $\eta_{ext}\Gamma_{sp}(N, p)$ normalized to $\eta_{ext}\Gamma_{sp}(N = 39, p = 18\ \mu\text{m})$ is plotted as a function of the grating period for the four distinct values of N. Several data points obtained for different mesas with identical geometry show very moderate dispersion of the measurements (full symbols), the origin of which lies in small shifts of emitted wavelength and slight positioning irreproducibility from sample to sample. Clearly, for a given cavity thickness, the experiment reveals peaked behavior with a maximum nearby $p = 16\ \mu$m, roughly on the second diffraction order of the grating for the wavelength 70 μm. While only slightly shifting to shorter periods, the maximum significantly increases when the cavity thickness is reduced.

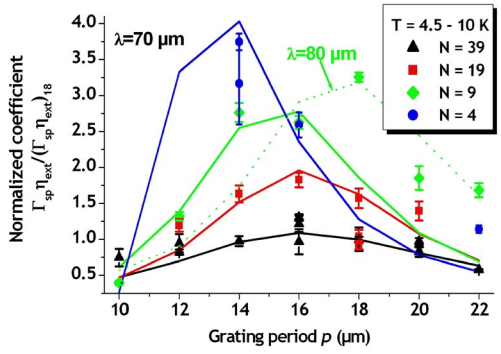

FIG. 3 (color online). Power extracted from the cavity as a function of the grating period, for four different cavity thicknesses: experiment (full symbols) and theory (solid lines). The theoretical curves are calculated at $\lambda = 70\ \mu$m, the dotted curve ($N = 9$) at $\lambda = 80\ \mu$m. The error bars are confidence intervals of the fitting procedure [Eq. (3)].

To interpret this behavior, the experimental results are compared to a theoretical model for the radiation emitted by a dipole source in a cavity, based on the modal method [13], upon surface impedance boundary condition. Details of the model can be found in Refs. [14,15]. In this framework both the product $\eta_{ext}\Gamma_{sp}$ and Γ_{sp} can be evaluated independently. To accurately obtain $\eta_{ext}\Gamma_{sp}$, the overall radiation in a cone with 120° opening around the grating normal is computed, and the spatial variation of the electromagnetic field inside the cavity is taken into account by averaging the radiated power over all the possible dipole positions.

As can be seen from Fig. 3, this model very satisfactorily accounts for the experiment, over a large span of cavity parameters p and L. In particular, the maximum of the extracted power as a function of the grating period p is correctly predicted, as well as the extracted power dependence on the cavity thickness L. The runaway data points can be explained by variation of the emission wavelength due to small variations of the thickness of the quantum wells across the wafer, as can be seen from the comparison of the data plot with the dotted line, computed for $N = 9$ and $\lambda = 80\ \mu$m.

Agreement between experiment and theory allows a reliable evaluation of the quantity Γ_{sp} and the Purcell enhancement factor f from the model, which yields [14]:

$$f = f_{cavity} + f_{grating} \quad (4)$$

for $f = \Gamma_{sp}/\Gamma_0$ with Γ_0 the free space SE rate. The first term f_{cavity} is the Purcell enhancement of a virtual planar cavity, in which the grating is replaced by a planar mirror. The second term $f_{grating}$ is the contribution of the grating. The numerical simulations show that, for the geometry of the samples, this contribution is negligible due to the screening effect of the doped contact layers. In fact f has almost identical values as those predicted by Eq. (1), which therefore can be used to estimate the Purcell effect in the devices, with L now being the active region thickness and n the undoped GaAs refractive index. This means that the guided TM modes propagating in the virtual cavity that are directly coupled to the vertical dipole are only weakly altered by the diffraction grating, and they benefit exclusively from the Purcell acceleration of the dynamics.

The Purcell factor f is then estimated in absolute value according to Eq. (4): $f = 4.2$ for $N = 39$ periods, and $f = 50$ for $N = 4$ periods, which is more than 1 order of magnitude enhancement as compared to a feedbackless device. Taking $n = 3.6$ and $\lambda = 73\ \mu$m, Eq. (1) gives a slight underestimate in the thinnest cavities: $f = 4.3$ for $L = 3.5\ \mu$m, and $f = 35$ for $L = 0.44\ \mu$m.

Moreover, the power enhancement observed experimentally cannot be attributed to an enhancement of the extraction efficiency η_{ext}. An estimate of this quantity can be obtained from the above model by using a TM guided

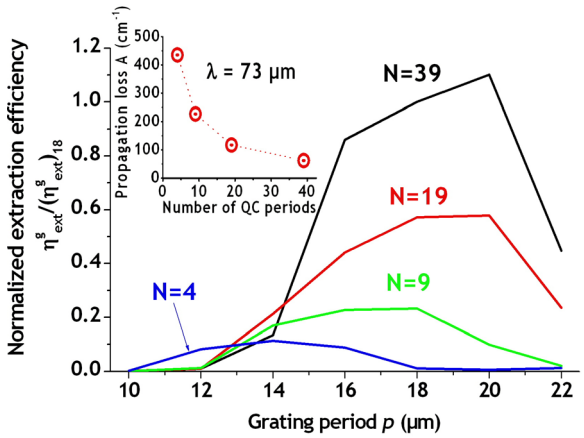

FIG. 4 (color online). Computed [Eq. (5)] extraction efficiency η^g_{ext} as a function of the grating period, for four different cavity thicknesses. Inset: propagation loss A vs the number of QC periods N ($\lambda = 73\ \mu$m).

cavity mode as a source term [16], instead of a localized dipole. Then the waveguide loss A_g due to diffraction is computed from the ratio of the vertical and horizontal components of the Poynting vector, and η^g_{ext} is provided by [16]:

$$\eta^g_{\text{ext}} = A_g/(A_g + A) \tag{5}$$

where A is the propagation loss due to absorption, mainly in the contact layers. Although not strictly equivalent, η_{ext} and η^g_{ext} are very related, since the TM-polarized dipole is emitting mainly in the TM (actually TM_0) guided cavity modes.

The quantity η^g_{ext} obtained for the guided mode propagating perpendicularly to the slits is plotted in Fig. 4, for comparison to Fig. 3. The same resonant behavior as a function of the grating period p is observed, which means that the p dependence of the product $\eta_{\text{ext}}\Gamma_{\text{sp}}$ is mostly contained in the η_{ext} factor. A striking feature of Fig. 4 is that the maximum extraction efficiency strongly decreases when the cavity thickness is reduced. Indeed, the computation shows that whereas A_g slightly decreases, the propagation loss A strongly increases because of increased overlap between the intracavity field and the absorbing contact layers (inset of Fig. 4). Therefore, a Purcell enhancement effect has to be invoked not only to explain enhancement of the maximum extracted power observed in the experiment (see Fig. 3), but also to compensate for the decrease of the extraction efficiency, due to absorption, when the cavity thickness is reduced.

In conclusion, subwavelength metallic cavities have been fabricated and studied using an MOCVD grown, THz-emitting quantum cascade as a source. The intersubband electroluminescence is out-coupled by a metallic grating deposited on the top of the device, which also serves as the upper cavity mirror. Theoretical analysis of the grating diffraction shows that the out-coupling efficiency drops with the device thickness, whereas the experimentally observed power per quantum cascade period rises when the thickness is reduced. The power enhancement is thus due to the Purcell effect, as confirmed by a an elaborate electrodynamical model for the dipole emission inside the grating-mirror cavity, based on the retro-action field. A Purcell factor of 50 is estimated for the thinnest device. To our knowledge, this is the first time Purcell effect is evidenced at THz frequencies with QC structures, which opens up perspectives to take advantage of cavity QED for higher radiative efficiency cavity devices in this frequency range. Indeed, in the present configuration, the Purcell effect is expected to occur even for a single laser mode, since the Purcell enhancement comes solely from the field confinement, and the cavity density of states is not involved.

The authors acknowledge support by the Région Ile de France and the Conseil Général de L'Essonne, P. Lalanne from Laboratoire Charles Fabry for a fruitful discussion, and G. Scalari from Université de Neuchâtel for the spectrally resolved measurements.

[1] E. M. Purcell, Phys. Rev. **69**, 674 (1946).
[2] P. Goy, J. M. Raimond, M. Gross, and S. Haroche, Phys. Rev. Lett. **50**, 1903 (1983).
[3] J.-M. Gérard, B. Sermage, B. Gayral, B. Legrand, E. Costard, and V. Thierry-Mieg, Phys. Rev. Lett. **81**, 1110 (1998).
[4] M. Pelton, C. Santori, J. Vučkovič, B. Zhang, G. S. Solomon, J. Plant, and Y. Yamamoto, Phys. Rev. Lett. **89**, 233602 (2002).
[5] O. Benson, C. Santori, M. Pelton, and Y. Yamamoto, Phys. Rev. Lett. **84**, 2513 (2000).
[6] G. Bourdon, I. Robert, R. Adams, K. Nelep, I. Sagnes, J. M. Moison, and I. Abram, Appl. Phys. Lett. **77**, 1345 (2000).
[7] S. Haroche, *Fundamental Systems in Quantum Optics* (Elsevier Science Publisher, Paris, 1992).
[8] R. Köhler, A. Tredicucci, F. Beltram, H. E. Beere, E. H. Linfield, A. G. Davies, D. A. Ritchie, R. C. Iotti, and F. Rossi, Nature (London) **417**, 156 (2002).
[9] M. Rochat, J. Faist, M. Beck, U. Oesterle, and M. Ilegems, Appl. Phys. Lett. **73**, 3724 (1998).
[10] R. Winston, J. Opt. Soc. Am. **60**, 245 (1970).
[11] M. Rochat, J. Faist, M. Beck, and U. Oesterle, Physica (Amsterdam) **7E**, 44 (2000).
[12] P. Hyldgaard and J. W. Wilkins, Phys. Rev. B **53**, 6889 (1996).
[13] L. Li, J. Mod. Opt. **40**, 553 (1993).
[14] Y. Todorov, I. Abram, and C. Minot, Phys. Rev. B **71**, 075116 (2005).
[15] Y. Todorov and C. Minot, J. Opt. Soc. Am. A **24**, 3100 (2007).
[16] B. Xu and Q. Hu, Appl. Phys. Lett. **70**, 2511 (1997).